Electrochimica Acta 462 (2023) 142785

Contents lists available at ScienceDirect

Electrochimica Acta

journal homepage: www.journals.elsevier.com/electrochimica-acta

Ionic transport in solid-state composite poly(trimethylene carbonate)–$Li_{6.7}Al_{0.3}La_3Zr_2O_{12}$ electrolytes: The interplay between surface chemistry and ceramic particle loading

Kenza Elbouazzaoui, Funeka Nkosi, Daniel Brandell, Jonas Mindemark *, Kristina Edström

Department of Chemistry – Ångström Laboratory, Uppsala University, Box 538, Uppsala SE-751 21, Sweden

A B S T R A C T

The ionic transport in solid-state composite electrolytes based on poly(trimethylene carbonate) (PTMC) with LiTFSI salt and garnet-type ion-conducting $Li_{6.7}Al_{0.3}La_3Zr_2O_{12}$ (LLZO) ceramic particles is here investigated for a range of different compositions. Positive effects on ionic conductivity have previously been reported for LLZO incorporated into poly(ethylene oxide) (PEO), but the origin of these effects is unclear since the inclusion of particles also affects polymer crystallinity. PTMC is, in contrast to PEO, a fully amorphous polymer, and therefore here chosen for the design of a more straight-forward composite electrolyte (CPE) system to study ionic transport. With LLZO loadings ranging from 5 to 70 wt%, the CPE with 30 wt% of LLZO exhibits the highest ionic conductivity with a cationic transference number of 0.94 at 60 °C. This is significantly higher than for the pristine PTMC polymer electrolyte. Generally, low to moderate LLZO loadings display a gradual increase of the ionic conductivity, transference number and also of the polymer-cation coordination number. The combined contributions of ionic transport along polymer-ceramic interfaces and Lewis acid-base interaction between the LLZO particles and the LiTFSI salt can explain this enhancement. With loadings of LLZO above 50 wt%, a detrimental effect on the ionic conductivity was however observed. This could be explained by agglomeration of ceramic particles, and by a partial coverage of LLZO particles with a Li_2CO_3 layer. Consequently, inner polymer-particle interfaces become more resistive, and Li^+conduction is prevented along interfacial pathways. The presence of Li_2CO_3 has more detrimental impact at higher LLZO loadings, since inter-particle connectivity will be hampered, and this is vital for efficient ionic transport. This suggests that there is an interplay between the LLZO particle surface chemistry with its loading, which ultimately controls the Li-ion transport.

1. Introduction

Solid-state batteries, in which the common liquid electrolytes are replaced with solid-state counterparts, are among the most promising candidates for future battery technology [1,2]. These are considered key components for the progress of next-generation batteries, granted that the solid electrolytes can provide similar or improved electrochemical performance as the liquid systems used today [3]. Solid electrolytes can generally be categorized into polymeric and inorganic materials. Polymer electrolytes are promising candidates thanks to their facile processing, fair mechanical strength and good interfacial contact with electrode materials, but their implementation in practical applications is held back due to their low intrinsic ionic conductivity, especially at room temperature or below [4–6]. Inorganic electrolytes, including oxides, sulfides, phosphates, and other alternatives, are better Li-ion conductors and many are also electrochemically and thermally stable, but are suffering from brittleness and poor interfacial contact with the electrodes. This, in turn, can generate high resistances and poor capacity [7–10]. Because of these drawbacks, solid electrolytes are still not being employed in commercial large-scale batteries to more than a limited degree [2,11,12]. During the last decade, the research community has devoted immense efforts to improve the performance and address the challenges faced by both polymeric and ceramic electrolytes [13–15].

Naturally, combining polymeric and ceramic materials into one ”composite” or “hybrid” electrolyte system constitutes an appealing strategy, aiming to merge the merits and overcome the respective problems of polymers and ceramics. This could in principle render high ionic conductivity ($\sim 10^{-3}$ S cm^{-1}), large electrochemical stability window, and good interfacial contact with the battery electrodes [16–19]. Nevertheless, this class of solid-state electrolytes has in practice not yet fulfilled this entire set of requirements [12,20,21]. In this context, intensive work has been centered around developing and investigating numerous composite electrolytes, often based on salt solutions in poly(ethylene oxide) (PEO) with various ceramic fillers. Two different approaches can be discerned depending on the ceramic loading: polymer-rich and ceramic-rich materials, where the filler concentration is below or above 50 wt%, respectively [22].

Since the mid-1970s, PEO has been a focal point in the field of solid polymer electrolytes (SPEs), emphasized after Armand showed Li^+-ion conduction in a matrix of PEO and a lithium salt [23,24]. Despite its

* Corresponding author.
E-mail address: jonas.mindemark@kemi.uu.se (J. Mindemark).

https://doi.org/10.1016/j.electacta.2023.142785
Received 12 April 2023; Received in revised form 12 June 2023; Accepted 24 June 2023
Available online 25 June 2023

inferior ionic conductivity as compared to liquid electrolytes at conventional battery operating temperatures, it is widely used as a polymer host in SPEs. Correspondingly, PEO-based systems are those that have been most extensively studied when fabricating polymer-ceramic hybrid electrolytes [25,26]. Several Li^+-ion conducting (garnet, NASICON, perovskite, argyrodite) and non-conducting (Al_2O_3, SiO_2, ZrO_2, etc.) inorganic fillers have been incorporated into a salt-containing (often LiTFSI) PEO-based polymer matrix, and the resulting composite electrolytes have been evaluated in terms of their ionic transport properties [27–34]. Generally, adding fillers to the PEO matrix reduces its degree of crystallinity, thereby maximizing the amorphous regions of the polymer matrix, in which the ionic transport occurs [26,29].

The garnet-structured $Li_7La_3Zr_2O_{12}$ (LLZO) oxide material has been given much consideration as compared to other inorganic fillers thanks to its ability to conduct lithium ions. A special focus has been attributed to the cubic LLZO phase because of its high bulk ionic conductivity at room temperature, explained by the particles densification and sintering at high temperatures (above 1000 °C). However, the brittleness of LLZO, interfacial issues with Li-metal, and chemical instability when exposed to air, still restrain its practical use as a solid electrolyte. Therefore, incorporating LLZO as a ceramic filler in solid or gel polymer electrolytes appears as a promising approach to overcome these problems [35,36].

Utilizing transport pathways through the LLZO bulk within a flexible polymer matrix constructs a primary motivation for incorporating such active fillers [10,37–40]. In this context, several papers have evaluated the ionic conductivity of PEO-LLZO composite electrolytes, and reported an enhancement resulting from suggested synergetic effects between the polymer and ceramic components in this hybrid system [29,34,41–47]. However, the specific ionic transport mechanisms in these composite electrolytes remain elusive, and it is unclear if the LLZO bulk contributes with any conductivity [48]. It could be considered that this lack of understanding constitutes a restriction for this class of solid-state electrolytes from reaching a major break-through, since it becomes difficult to design and tailor them for optimal performance. Therefore, it is necessary to better explore the fundamentals behind the ionic conduction behavior in LLZO-based hybrid electrolytes.

It is noteworthy that while the theories of the ionic transport mechanism in both polymer and ceramic electrolytes are fairly well established, only few insights on the potential mechanism have been proposed for the widely explored PEO-LLZO composite electrolytes. In SPEs, the conduction mechanism conventionally takes place in amorphous regions by segmental motion of polymer chains according to a Vogel-Fulcher-Tammann (VFT) behavior above T_g [49]. When the chains undergo segmental motion into a free-volume space, the Li^+ cations coupled to the polymer coordinating groups migrate within the polymer matrix. Li^+ conduction in inorganic solid electrolytes, on the other hand, occurs by ion-hopping through interconnected fixed sites in the host structure and is dependent on connected percolating pathways, and the ionic conductivity thereby follows an Arrhenius-type behavior rather than VFT [10].

For solid polymer-ceramic composite electrolytes, there is no general consensus on the conduction mechanism, and it seems dependent on several factors: polymer hosts, nature and loading of the ceramic filler, Li-salt concentration, etc. In the studies of PEO-based composite electrolytes, it has then been demonstrated that the transport mechanisms are strongly dependent on phase changes occurring in the polymer phase of the system, thereby affecting the overall ionic conductivity. Three distinctive conduction modes have been suggested: (i) in the polymeric phase, where the dispersed ceramic particles decrease the polymer crystallinity, contributing to an increase of the amorphous regions where the conduction generally occurs; (ii) in the inorganic phase, bulk conduction can also contribute to the total conductivity of the hybrid system if the ceramic fillers are active and the particle loading is high; (iii) at the polymer-ceramic interfaces formed, which can provide an additional transport pathway. The motivation for using LLZO and similar active fillers primarily comes from the addition of conduction mode (ii), but in practice mode (iii) has often been ascribed as the main factor behind to the significant conductivity enhancement observed. However, it has also been found that the interfacial resistance in the well-studied PEO-LLZO system is even larger as compared to the resistance at the polymeric and ceramic phases, and should thus limit the conductivity [50].

In the efforts of exploring the conduction mechanisms in this category of materials, it is useful to include also other polymer hosts than PEO, and evaluating the transport mechanisms in such systems could be a crucial step towards a better understanding of how composite electrolytes function in a battery cell. In this context, it is noteworthy that suppressing the polymer crystallinity after ceramic addition is not attainable with fully-amorphous polymer matrices, and eliminating this effect can contribute to a better understanding of other transport-controlling phenomena. One such interesting amorphous polymer host is poly(trimethylene carbonate) (PTMC) that, despite its limited conductivity, has been extensively studied as a battery electrolyte [4,30,51]. As PTMC is a fully-amorphous polymer, the effect of lowering crystallinity that is seen in PEO-based composite electrolytes would not be present, thereby isolating the intrinsic effects of the combination of LLZO with the polymer matrix.

Hence, the effect of LLZO concentration on the conduction properties of a series of composite electrolytes based on a PTMC-LiTFSI matrix and LLZO ceramic filler throughout a large range of ceramic filler contents (from 5 until 70 wt%) is here investigated. The ionic conductivity is correlated to the polymer-ion interactions as a function of the ceramic LLZO loading. In contrast to much work in the solid-state electrolyte field, this study does not focus primarily on improving the ionic conductivity of these PTMC-based electrolytes with ceramic incorporation, but rather to provide insights into what controls the ionic transport mechanisms in these hybrid electrolytes.

2. Experimental

2.1. Materials

Trimethylene carbonate (TMC; Richman Chemicals), stannous 2-ethylhexanoate (95%; Sigma-Aldrich) and dry toluene (99.8%; Acros Organics) were stored and handled in an argon-filled glovebox. Lithium bis (trifluoromethylsulfonyl)imide (LiTFSI; BASF) was dried at 120 °C under vacuum in a Buchi oven for 48 h prior to use. Li_2CO_3 (99.99%), La $(OH)_3$ (99.99%), and ZrO_2 (99%) purchased from Sigma-Aldrich, and Al_2O_3 (99.9%; VWR) were the main precursors for LLZO synthesis, and were used as received. Anhydrous acetonitrile (99.8%; Sigma-Aldrich), 1-propanol (>99.5%; Sigma-Aldrich), and lithium foil (125 μm; Cyprus Foote Mineral Co.) were also used as received.

2.2. Synthesis of $Li_{6.7}Al_{0.3}La_3Zr_2O_{12}$ particles

Abbreviated as “LLZO”, the cubic phase of the garnet-type ceramic was synthesized following a classic solid-state synthesis route [52]. Stoichiometric amounts of raw materials (Li_2CO_3, $La(OH)_3$, ZrO_2 and Al_2O_3) were mixed, to which 1-propanol was added and placed inside a zirconia jar for wet ball-milling using zirconia balls at a speed of 450 rpm for 12 h in a planetary ball-mill instrument (Retsch PM100). 10% excess of Li_2CO_3 was added to the previous mix to compensate for Li loss during sintering at high temperatures. The obtained white mixture was placed in an Al-crucible and dried inside a ventilated oven at 80 °C for 4–6 h to remove any solvent residues prior to heat treatment. The sintering was conducted in a muffle furnace (MTI corporation, VBF1200X) from room temperature up to 1000 °C for 12 h in air with a rate of 2 °C/min applied during both heating and cooling. The resulting powder was thereafter ball-milled again following the same above-described procedure and stored immediately inside an argon-filled glovebox before use.

2.3. Synthesis of poly(trimethylene carbonate)

High-molecular-weight PTMC was synthesized through bulk ring-opening polymerization of trimethylene carbonate catalyzed by tin(II) 2-ethylhexanoate according to a procedure previously described in detail by Sun et al. [51]. Briefly, in a stainless steel reactor 0.2 mol of TMC was added to 0.04 mmol of $Sn(Oct)_2$ (40 μL of 1 M solution) as catalyst in dry toluene. The reactor was sealed under argon atmosphere, then placed in an oven at 130 °C for 72 h. The reactor was shaken regularly every 30 min for the first 3 h to ensure a good mix of all constituents. Once the polymerization was complete, the reactor was put back inside an argon-filled glovebox and the final product was removed and cut into small pieces. The obtained polymer was a transparent and rubbery solid, with an approximate molecular weight M_w of 380 000 – 400 000 g mol^{-1} (confirmed by GPC).

2.4. Solid polymer electrolyte and PTMC/LLZO composite electrolytes preparation

Self-standing polymer and composite electrolyte films were obtained via a controlled solvent evaporation solution-casting method. Firstly, 72 wt% PTMC and 28 wt% LiTFSI salt were mixed and dissolved in acetonitrile ([Polymer]/[Solvent] = 0.05 g/ml) and kept under magnetic stirring at 40 °C for 12 h inside the glovebox. The resulting solution was poured into Teflon molds before being transferred inside a vacuum oven at a temperature of 30 °C and a pressure of 200 mbar for the first 20 h. Subsequently, the temperature increased up to 60 °C while the oven was further pumped down to <2 mbar for the next 40 h. After cooling, the obtained SPE films were punched using a 15 mm in diameter punching tool. All process steps were performed inside an argon-filled glovebox and the as-prepared electrolyte films were used as obtained.

Polymer-ceramic composite electrolytes with a nominal composition of (1-x) wt% [PTMC – 28 wt% LiTFSI] – x wt% LLZO ($5<x<70$) were prepared via a two-step process. Firstly, both PTMC and LiTFSI were dissolved in acetonitrile at 60 °C for 12 h. The ratio of polymer to solvent was 0.1 g mL^{-1}. The obtained solution was relatively viscous to facilitate the impregnation of ceramic particles into the polymer matrix and avoid sedimentation . Subsequently, appropriate amounts of the polymer+salt solution and LLZO powder were placed in a zirconia jar and ball-milled at 25 Hz for 15 min under argon atmosphere. The homogeneous polymer-salt-ceramic slurry was solution-cast in Teflon molds, and the solvent was evaporated using the same method as previously described above. Similarly, the composite polymer electrolyte ("CPE") films were punched out with a 15 mm in diameter puncher, and their thicknesses were measured with a Mitituyo digital indicator micrometer with typical values ranging from 50 to 250 μm depending on the ceramic concentration in the composite electrolyte samples. The entire procedure was performed inside an argon-filled glovebox prior to cell assembly and characterization.

2.5. Cell assembly

The as-synthesized SPE and CPE films were hermetically placed in CR2025 coin cells, sandwiched between two blocking stainless-steel electrodes with a Teflon spacer ring and pressed inside an argon-filled glovebox before being taken out for measurements. This configuration was employed for ionic conductivity experiments.

Prior to transference number measurements, Li/electrolyte/Li configuration-type pouch cells were fabricated. First, Li-metal disks were cut using 13 mm and 15 mm in diameter punchers. The cells were assembled by placing the CPE film between two Li-metal disks, and sealed afterwards using a vacuum sealer. All steps were carried out in an argon atmosphere.

2.6. SPE and CPE characterization

The total ionic conductivity of the SPE and different CPEs was determined by electrochemical impedance spectroscopy (EIS). The assembled coin cells were firstly annealed at 90 °C for 1 h and then left to cool down to room temperature prior to measurement to ensure good contact between the electrolyte film and the blocking electrodes. Thereafter, the experiments were carried out in the frequency range 7 MHz – 100 mHz with an amplitude of 50 mV at temperatures ranging from 30 to 90 °C using a Schlumberger SI 1260 impedance/Gain-Phase analyzer. All cells were kept for 1 h at each temperature to equilibrate before measurements. The impedance data were treated and fitted to a Debye circuit for the SPE and CPEs with 5 and 10 wt% of LLZO particles, and to another equivalent circuit (described in Fig. S1) for composite electrolytes with a ceramic concentration above 10 wt%. The bulk and polymer-ceramic interface resistances were determined after fitting in Zview v.3.3b (Scribner Associates), and the total ionic conductivity σ was calculated using the equation:

$$\sigma = \frac{l}{RA} \tag{1}$$

where l is the thickness, R is the bulk resistance for the SPE, or the sum of the bulk and internal interfacial resistances for the CPEs, and A is the cross-section geometrical area of the electrolyte film.

The Li^+ transference number was determined through the Bruce-Vincent method. The assembled pouch cells were first kept under open-circuit voltage conditions at room temperature for 24 h before setting the temperature at 60 °C for the measurements. The experimental procedure was conducted using a BioLogic SP-240 Potentiostat, and consisted of two steps: impedance spectroscopy and potentiostatic polarization. The measurements were carried out between 7 MHz and 10 mHz with an amplitude of 10 mV and a bias of 0 and 10 mV before and after polarization, respectively. Thereafter, the bulk and interface resistances were determined by fitting to an appropriate equivalent circuit illustrated in Fig. S2, using EC-lab software, while the initial current was calculated from the applied polarization potential and the total resistance in the cell. The cationic transference number was then calculated from the following equation:

$$T^+ = \frac{I_{SS}(\Delta V - I_0 R_0)}{I_0(\Delta V - I_{SS} R_{SS})} \tag{2}$$

where ΔV is the applied polarization voltage, I_0 and R_0 are the initial current and resistance, respectively, and I_{SS} and R_{ss} are the steady-state current and resistance, respectively.

To investigate the ion coordination properties, Fourier-transform infrared spectroscopy (FT-IR) experiments were carried out using a PerkinElmer Spectrum One FT-IR spectrometer equipped with a ZnSe crystal attenuated total reflectance (ATR) setup at room temperature. FT-IR spectra were recorded from 4000 to 650 cm^{-1} with a 4 cm^{-1} resolution and the peaks of interest were deconvoluted using the Voigt function after a linear baseline correction in the Origin software. The measurements were performed at least three times for reproducibility and accuracy. Each sample was kept inside a hermetically sealed argon-filled transfer box and taken out directly before starting the measurements to minimize air exposure.

The crystal structures of LLZO and PTMC-LLZO CPEs were confirmed through X-ray diffraction using a Bruker D8 Advance diffractometer. The XRD patterns were recorded over a 2θ range of 10–70° and employing Cu Kα radiation (λ = 1.54178 Å) as the main X-ray source. The CPE morphology, the ceramic particle distribution in the polymer matrix, and elemental composition were evaluated by scanning electron microscopy using a Zeiss Merlin SEM coupled to an energy-dispersive X-ray spectroscopy (EDS) detector. Top SEM images were acquired with an applied acceleration voltage of 3 kV, a 100 pA probing current, a ~6.3 mm working distance, and a secondary electron detector. The samples

were prepared under argon atmosphere and transferred inertly to the SEM microscope through a vacuum-sealed transfer box, designed to ensure transfer under inert conditions.

Surface analysis of the as-synthesized LLZO powder was performed by X-ray photoelectron spectroscopy (XPS). Firstly, a small quantity of the powder was placed and pressed on top of copper tape. The sample was prepared under argon atmosphere and brought to the XPS loading chamber through an airtight transfer shuttle without being exposed to ambient air. XPS characterization was carried out on a Kratos Axis Supra+ spectrometer with a monochromatized Al Kα ($h\nu = 1487$ eV) X-ray source, corresponding to a probing depth of ~10 nm. An electron neutralizer was also involved during measurements to compensate for over-charging. All spectra were collected with an emission current of 15 mA and the pressure in the analysis chamber was $\sim 2.6 \times 10^{-8}$ mbar. The elemental peaks of interest (La3d, Zr3d, C1s) were measured before and after surface etching, after obtaining a general survey spectrum. Surface etching was performed by monoatomic Ar^+sputtering, through which Ar gas is directly fed into the ionization chamber producing an Ar^+-ion beam with an energy of 500 eV to 8 keV. The beam allowed sputtering thin layers off the sample surface. Sputtering sequences of 60 s were employed 5 times. Spectra were recorded after each sputtering step and comparisons were made between the pristine and etched surfaces.

3. Results and discussion

Poly(trimethylene carbonate) (Fig. 1) is a fully amorphous polycarbonate, which can be used to fabricate solid polymer electrolytes thanks to its ability to coordinate cations by its carbonyl groups [51]. It has previously not been studied as a polymer matrix for solid composite electrolytes with ceramic fillers. The fact that PTMC is amorphous renders it particularly useful to investigate fundamental transport mechanisms, since the addition of fillers will not affect the polymer crystallinity, as is the case for PEO and other semi-crystalline SPE hosts, and which makes it more difficult to distinguish the causes for variations in ionic transport. This work thereby focuses on investigating the ionic transport in hybrid electrolytes based on a PTMC-LiTFSI matrix with LLZO as a potentially active ceramic filler. To ensure mechanical stability of the films before and after filler addition, high-molecular-weight PTMC was synthesized and employed, with a number-average molecular weight ranging approximately between 368 000 and 400 000 g mol^{-1}. The obtained polymer batch was a rubbery-like transparent solid, to which 28 wt% LiTFSI was added to form a polymer-salt matrix. The [Li^+]:[Carbonate] ratio was kept constant for the entire study, and was chosen based on previous work reporting the optimal ionic conductivity with LiTFSI content ranging between 25 and 30 wt% [53,54]. An SPE reference consisting of only PTMC with 28 wt% LiTFSI was likewise prepared.

To the PTMC-LiTFSI matrix, LLZO particles were added to produce composite electrolyte films with different ceramic loadings in the range of 5 to 70 wt% (denoted CPE5 – CPE70). Firstly, the crystal cubic structure of LLZO was confirmed by X-ray diffraction, and only minor appearance of secondary phases (<5%) could be detected. Similar XRD patterns were obtained for the CPEs, well displaying the characteristic peaks of cubic LLZO and thereby verifying the chemical stability of LLZO after being incorporated into the polymer matrix and ball-milled prior to casting for all compositions. The amorphicity of PTMC was also confirmed through the gaussian-shape XRD pattern obtained for the PTMC-based SPE, as shown in Fig. 2a.

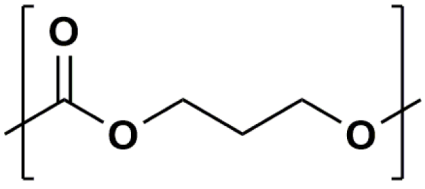

Fig. 1. Structure of poly(trimethylene carbonate).

To investigate the polymer stability and if the addition of ceramic filler had any significant effect related to structural changes in the polymeric matrix, FTIR was employed. The characteristic vibrations of PTMC could be observed both before and after adding the Li-salt and the LLZO ceramic filler. As illustrated in Fig. 2b, the symmetric carbonyl stretching vibration of neat PTMC is usually seen at 1741 cm^{-1}, which is sensitive to Li^+-cation coordination. Therefore, the carbonyl vibration shifts to lower wavenumbers upon addition of salt, resulting in two vibrations assigned to free and Li^+-coordinated carbonyl groups (as discussed in more detail below).

When discussing the effect of ceramic particles loading on the ionic conduction behavior of these CPEs, we first categorize the entire series based on the particle content. Thereby, a polymer-rich series is here defined when the LLZO content is below 50 wt%, where the ceramic primarily would contribute to the creation of novel Li^+-ion transport pathways along polymer-ceramic interfaces. When the LLZO content is at and above 50 wt%, the polymer could instead act as binder that is filling the gaps between the ceramic particles, and contribute to the formation of a continuous particle network; thus defining a ceramic-rich series of composite electrolytes. It should be noted that these definitions are based on the filler loading by mass and not by volume, which is also the case for most studies in literature [18]. The volume percentages of the entire series of this study are listed in Table S1 and range from ca. 1.3 vol% to 37.5 vol% for the materials studied here.

The ionic conductivities of the as-synthesized CPEs and the SPE reference were investigated by electrochemical impedance spectroscopy, using 15 mm diameter electrolyte films of a thickness varying from 50 to 190 μm with increasing the ceramic content. The Nyquist plot of the SPE without ceramic particles displayed a typical behavior of an SPE as shown in Fig. 3, with a regular semi-circle at high frequencies attributed to the polymer bulk conduction, followed by a spike at medium and low frequencies. A similar Nyquist plot was obtained for the CPE with 5 wt% of LLZO, indicating that the introduction of such a small fraction of ceramic particles did not bring any noticeable effect on the main transport mechanism. Starting from CPEs with 10 wt% of LLZO, a novel feature appeared at medium frequency ranges. The shape of the Nyquist plots showed two depressed semi-circles at high and medium frequencies, followed by a straight line at low frequencies. With increasing ceramic loading in the polymer matrix, this feature became more pronounced and its resistance appeared to be higher as compared to the bulk resistance as seen in Fig. S1. Through comparisons with the SPE reference, it is suggested that the first semi-circle for the CPEs is attributed to the polymer bulk conduction, while the second is assigned to the polymer-ceramic interfaces in the system. The absolute value of impedance as function of the frequency was plotted in a Bode-type plot in Fig. S2, and confirmed the appearance of two distinctive phenomena at high and medium frequency range for CPEs with a ceramic loading equal or above 10 wt%. Therefore, both bulk and interfacial resistances (R_b and R_{int}, respectively) were taken into consideration when calculating the ionic conductivity in these samples, while only the bulk resistance R_b was used for SPE and CPE5 samples. To verify reproducibility and report reliable data, we have performed the analysis on at least 3 cells for each composition from the entire series, and observed minor differences in total resistance values between different samples from the same composition.

Appropriate equivalent circuits were proposed and employed to fit the data and determine the resistance values for each material. For SPE and CPE5, a typical Debye circuit was used, while another circuit consisting of two R/constant phase elements in series was suggested for the best fit for the other samples, as illustrated in Fig. S3. To confirm that the high and medium-frequency features observed in the Nyquist plots correspond to bulk and interfacial responses respectively, the capacitance values obtained after fitting were evaluated. For the SPE and CPE5

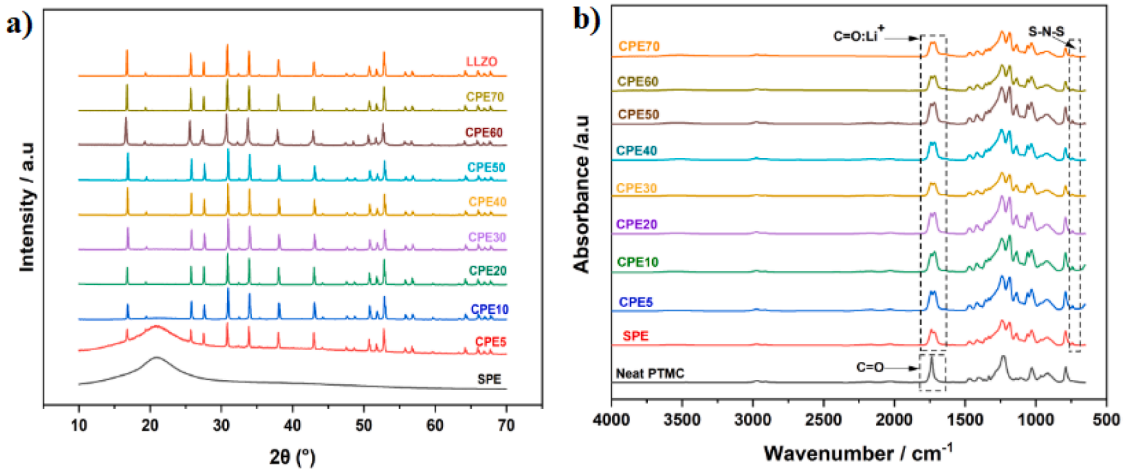

Fig. 2. (a) X-ray diffraction patterns of filler-free solid polymer electrolyte (SPE), composite electrolytes (CPEs), and pristine LLZO powder; (b) FTIR spectra of SPE, CPEs, and pristine PTMC polymer.

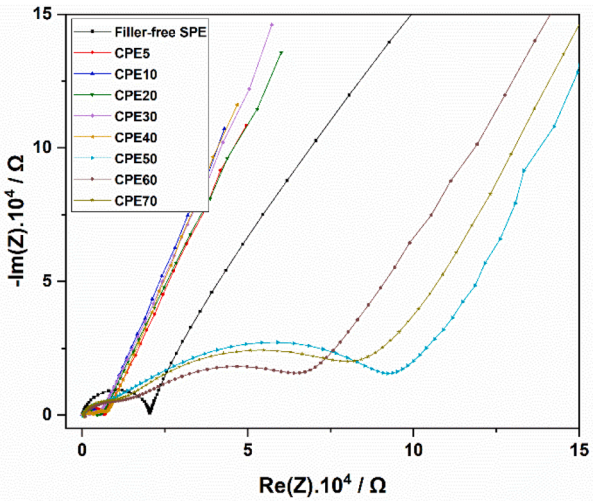

Fig. 3. Electrochemical impedance spectroscopy measurements of SPE and CPE electrolytes from 7 MHz to 100 mHz: Nyquist plot of SPE and CPEs at 60 °C.

samples, capacitance values in the order of 10^{-9}–10^{-10} F cm^{-2} were obtained, considered as typical values of the bulk capacitance of the sample. Therefore, the first semi-circle at high frequencies can indeed be associated to the conduction phenomena occurring in the polymer bulk. For CPEs with LLZO content above 5 wt%, fitting data displayed similar capacitance values assigned to the high frequency semi-circle as for SPE, and capacitance values in the order of 10^{-8}–10^{-7} F cm^{-2} were attained for the following semi-circle, that can be assigned to conduction feature along the interfaces between polymer and ceramic in the CPEs [55].

The obtained impedance spectra for the PTMC-based CPEs display striking differences as compared to those for similar materials based on PEO. Here, the additional feature of an incomplete depressed semi-circle in the medium-frequency region can clearly be observed, while PEO-LLZO composites generally exhibit one single semi-circle at high frequencies. Samsinger et al. attributed this signal to the bulk resistivity, claiming that there was no observed feature for the polymer-ceramic interface [56]. On the other hand, Kato et al. suggested that the Li^+-conduction can possibly occur in the LLZO phase and near the interfaces [57].

The total ionic conductivity as a function of temperature for different composite electrolytes and the SPE reference is plotted in Fig. 4a. As can be seen, all samples display a VFT behavior within the entire tested temperature range, indicating that the ionic conduction occurs primarily coupled to the segmental motion of the polymer chains. For the polymer-

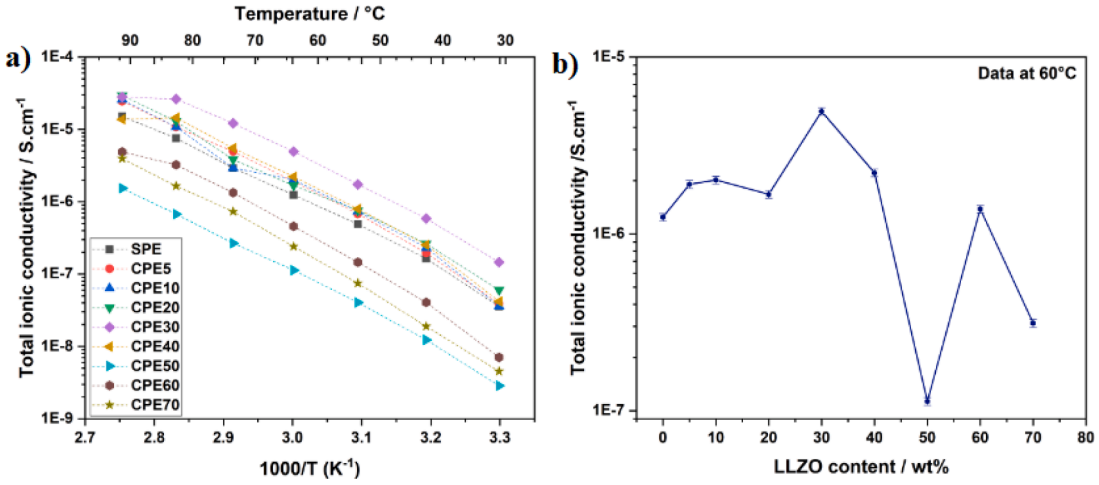

Fig. 4. (a) Arrhenius-type plots of the total ionic conductivity of SPE and CPEs from 30 to 90 °C within the entire range of LLZO concentration; (b) Li-ion conductivity as function of the ceramic LLZO concentration at 60 °C. Standard error of the mean is represented as error bars.

rich materials, it is clearly seen that the ionic conductivity is higher with incorporation of active ceramic filler as compared to the electrolyte without LLZO particles; i.e., all curves are above that of the SPE reference. The conductivity increases with increasing ceramic contents up to 30 wt% of LLZO, after which the conductivity is observed to drop significantly, especially for samples with LLZO loadings of 50 wt% and above. This is also seen in Fig. 4b, which shows the trend specifically for 60 °C. This conductivity trend can be due to several factors. Firstly, the incorporation of a small LLZO fraction could increase the Li mobility through enhancing the Li solvation in the system. This can be explained by a Lewis acid-base interaction between the ceramic particles and the salt anions, leading to an increased supply of mobile lithium cations. Secondly, the ceramic particle concentration can significantly affect the conductivity in CPEs negatively if agglomerates are formed in the conductive SPE matrix, corresponding to obstacles which can hinder Li-ion transport pathways through the polymer matrix. Finally, inner polymer-ceramic interfaces are likely to play a key role for the conductivity in CPEs. While such interfaces are often argued to provide useful transport paths for the mobile cations and promote conductivity, it has also been reported that such interfaces can be quite resistive and thereby restrict lithium ion transport along them [58].

It is not straight-forward to explain the conductivity trends seen in Fig. 4. As can be seen from the Nyquist plot (Fig. 3), the observation of a second semi-circle at the medium frequency range indicates a contribution of the polymer-ceramic interfaces to the total ionic conductivity for CPEs with LLZO contents at and above 10 wt%. When the 'optimal' LLZO content is exceeded (at ca. 30 wt% here), there is an increase in the bulk ionic resistance (Fig. S4). This is likely related to the increased tortuosity for ion transport through the polymeric phase as more pathway-blocking particles are added. Even more striking, however, is the drastic increase in interfacial resistance when the LLZO content reaches 50 wt%, leading to a huge drop in overall conductivity. At this point, it is not clear why this particular particle concentration gives such a huge interfacial resistance, but it is consistently observed in our samples. Particle agglomeration could be one possible answer, and agglomerates are clearly seen in SEM imaging (see Fig. S5). Moreover, the agglomeration can lead to that the particle surface area that is exposed to the polymer stops to increase with particle loading. This might also be correlated to that the surface chemistry of the LLZO particles plays a role, since these can be partially covered by Li_2CO_3 (discussed below), which is more resistive than the bare LLZO substrate. If the LLZO-LLZO contacts are preferred during agglomeration, it would lead to an increased fraction of the poorly conductive surfaces on behalf of the well-conducting bare LLZO, and can thus partly explain the observed trends.

An increase in the ionic conductivity of CPEs with high LLZO loadings (above 50 wt%) could also be expected due to contributions from LLZO bulk conduction. However, our data display the opposite trend for these PTMC-LLZO CPEs, with a drastic decrease in conductivity starting from 50 wt% of LLZO. We also observe agglomerates at these loadings, which highlights the insulating nature of the bulk LLZO in our CPEs.

To better elucidate the effect of active ceramic filler content on the ionic conduction properties of PTMC-based electrolytes, it is vital to investigate the coordination chemistry of the cations, and how this depends on the electrolyte composition. There is plenty of evidence in literature that the ion-polymer coordination strongly influences the ionic transport properties in SPEs. The cation solvation structure, which in SPEs is dominated by the interaction with the functional groups of the polymer, is likely to change when a third component (the ceramic particles) is introduced. It can be envisioned that this occurs either through modifications of certain polymer-salt interactions as a result of the chemical interplay between the polymer and the particles, or that the particles are acting as anion immobilizers through Lewis acid-base interactions with the salt. In polycarbonate-based polymers, the interaction with lithium cations results in the observation of two bands in the vibrational spectra which correspond to free functional groups and Li^+-coordinating groups [59,60]. For polycarbonate-based polymers, both FTIR and Raman spectroscopy has been used to explore the coordination chemistry of both polyethylene carbonate (PEC) [61,62] and PTMC for both Li-based [63] and Na-based systems [54].

In PTMC-based electrolytes, the Li cations coordinate to the C = O groups. The FTIR C = O symmetric stretching vibration in neat PTMC can be observed at ~1740 cm^{-1}, but – as seen in Fig. 2b – is split and shifted to lower wavenumbers with the addition of lithium salt and LLZO particles. The coordinating carbonyl groups can be assigned to the peak at ~1715 cm^{-1}. By deconvolution of the C = O doublet into two peaks, assigned to coordinating and non-coordinating groups (illustrated in Fig. 5a), the fraction of either C = O type can be quantified from the peak area.

The obtained ratio here of [C = O:Li^+]:[C = O]= 58:41 for the PTMC-based SPE without fillers is in good agreement with what has previously been reported for the same system, with some minor differences due to differences in salt concentration [63].

The cation coordination number to the polymer was calculated as $CN = \chi \times n$, where χ is the obtained percentage of Li^+-coordinating carbonyl groups after deconvolution, and n is the [C = O]:[Li^+] molar ratio (kept constant at $n = 7.23$, equivalent to a salt concentration of 28 wt%). The calculation was made assuming equity between the extinction coefficients for non-coordinating and coordinating carbonyl groups in the system. Fig. 5b shows the variation of the coordination number with LLZO content with the corresponding data in Table S2, while all deconvoluted FTIR peaks can be found in Fig. S6. It is apparent that the polymer continues to complex the Li ions also in the presence of ceramic particles, while there is no evidence on any interaction between the polymer and the particles, as is seen in Fig. S7. Comparing the spectra of neat PTMC and the salt-free samples containing PTMC and LLZO only, we can observe the same single peak attributed to the free carbonyl group vibration. The fraction of coordinating carbonyl groups in fact increases with increasing ceramic loadings, with some small exceptions (e.g. CPE20, which also is an outlier in terms of conductivity; see Fig. 4). The Li^+-carbonyl coordination number increases with the ceramic concentration all the way up to 70 wt%. This suggests that the ceramic particles have an interaction with the lithium salt, primarily through an interaction between the anions from the salt acting as a Lewis base and the ceramic particles acting as a Lewis acid that can accept electron pairs via La^{3+} or Zr^{4+}. As a result, Li-salt dissociation is promoted, which could also render a decrease in the anionic mobility. An increased number of 'free' lithium charge carriers (not ion-paired) is thereby likely to be obtained, thus enhancing the polymer coordination number. Assuming that Li^+ dissolution and coordination to the mobile polymeric solvent can contribute to enhance the ionic conductivity in polymer electrolytes, this can explain the conductivity trends observed for lower ceramic contents (up to CPE30). However, a drastic decrease in ionic conductivity can still be observed at and above 50 wt% loading, despite an increase of the coordination number. This trend at higher loadings cannot be explained by any ionic coordination-ionic conductivity relationship, but rather by the agglomeration of particles in the SPE matrix, resulting in a blockage of ionic transport paths.

In addition to interactions between lithium cations and the polymer functional groups, Li^+ ions can also coordinate to the TFSI anions leading to the formation of ion pairs and clusters. This can significantly affect the conduction properties of the overall PTMC-based system, either positively or negatively [64]. Despite sometimes leading to a higher transference number, ion pairing generally remains detrimental in SPEs and CPEs, limiting the fraction of available free cations to be coordinated to the polymer functional groups.

In the analysis of the ion paring of in these systems, we focused on the polymer-rich series up to 50 wt% of LLZO, due to the complexity of fitting these multi-components systems at higher loadings. As shown in Fig. 2b, a broad peak appears in the region 740–750 cm^{-1}, assigned to the S-N-S vibration of the TFSI anions. This same feature was seen for all CPEs, and was deconvoluted in order to quantify the ratio of free anions

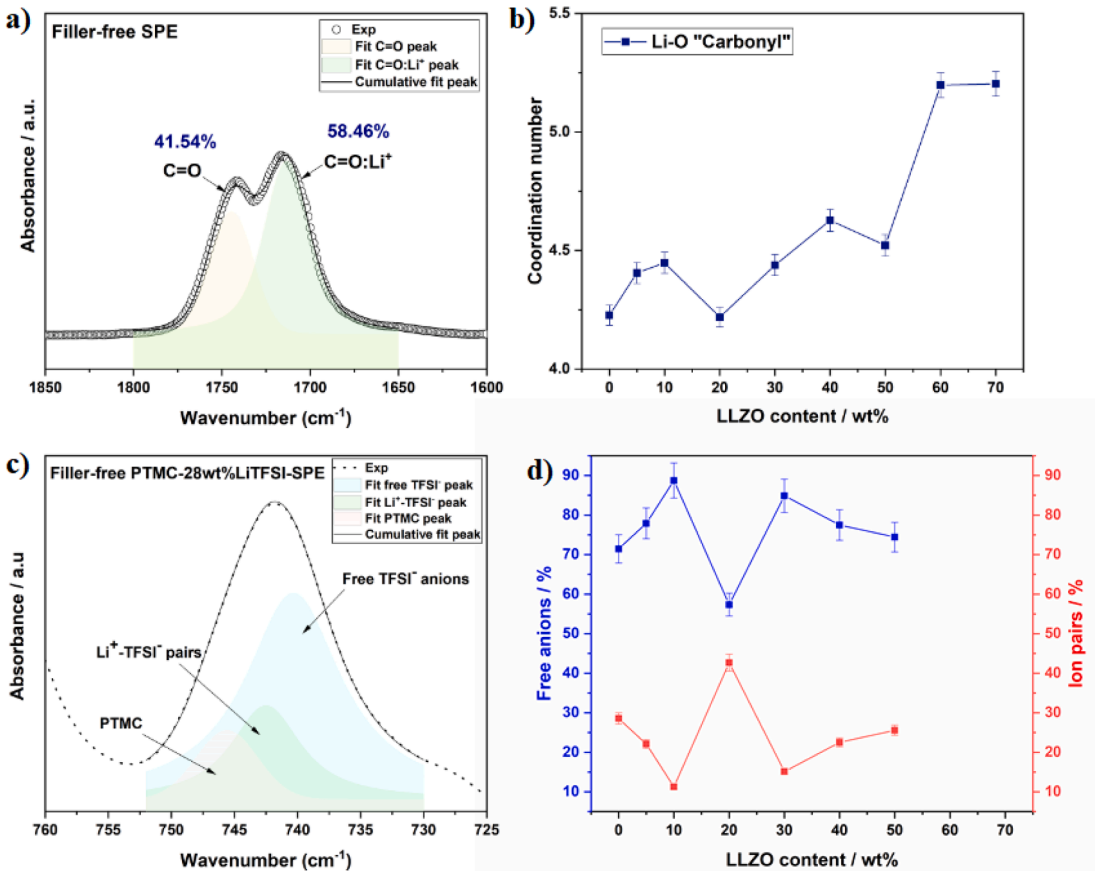

Fig. 5. (a) Deconvoluted FTIR spectra of an SPE without ceramic particles in the 1850–1600 cm^{-1} region; (b) Coordination number vs. ceramic concentration; (c) Deconvoluted FTIR spectra of an SPE in the 760–725 cm^{-1} region. The peaks at 740 and 745 cm^{-1} are assigned to free ions and ion clusters respectively, and the continuous black and dashed lines represent the sum of the fitted peaks and the experimental data respectively; (d) Portion of free ions and ion pairs vs. LLZO loadings for the polymer-rich series. Standard error of the mean is represented as error bars.

to ion pairs (Fig. S8). The "Li-TFSI" ion pair peak is shifted and seen at ~745 cm^{-1}, while the "free" anions peak remains at 740 cm^{-1}. Deconvoluting the FTIR spectra in this region is challenging because of interference from a third peak, attributed to C—H bending vibration in the polymer (see Fig. S9). Therefore, this additional component was taken into consideration during deconvolution where equity between extinction coefficients was assumed prior to calculation of the fraction of free anions and ion clusters (see Table S3 for more details).

As seen in Fig. 5d, the fraction of free anions and ion pairs display the reverse trend. Assuming that the number of free TFSI anions is correlated to free Li cations in the system, this would correspond to an increase of the fraction of free lithium cations up to 30 wt% ceramic loading, while a slight decrease of this fraction is observed starting from 40 wt% of LLZO. The observed increase in the portion of free charge carriers up to 30 wt% of LLZO is in good agreement with the increase seen in the total ionic conductivity of CPEs up to 30 wt%. In addition, it

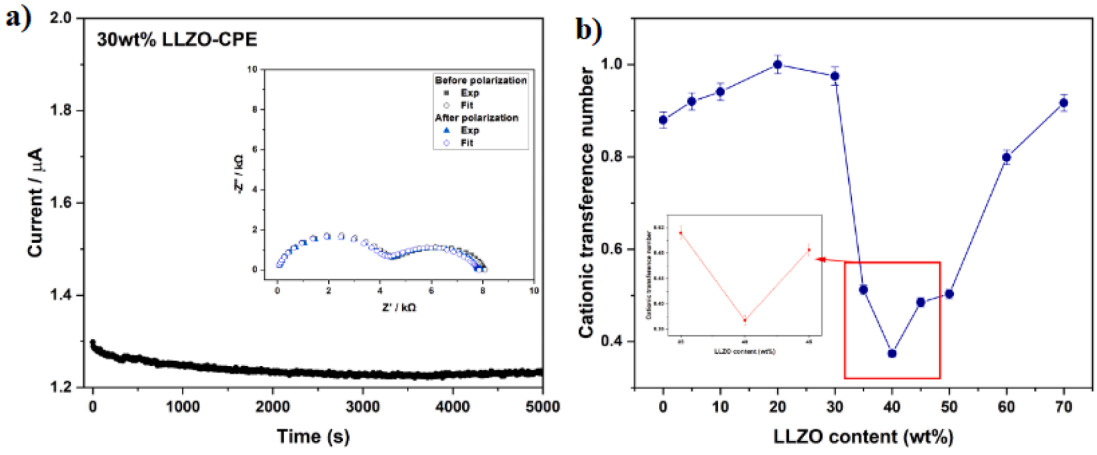

Fig. 6. (a) Chronoamperometric response of a Li/CPE30/Li symmetrical cell at 60 °C. Inset: Nyquist plot before and after polarization; (b) Variation of the cationic transference number as function of LLZO ceramic concentration. Inset: T_+ variation from 35 to 45 wt% of LLZO. Standard error of the mean is represented as error bars.

seems that the free ions and ion pairs portions for CPES with 40 and 50 wt% of LLZO are more or less similar to the initial amount detected for the filler-free SPE. This could be due to an interaction between F^- from TFSI anions with La^{3+} or Zr^{4+} upon addition of LLZO particles, which explains the decrease of ion pairs portion for CPEs up to 30 wt%. However, this interaction seems to be less pronounced for CPEs with 40 and 50 wt% of LLZO, which can be speculated to be due to any changes for the LLZO surface chemistry (more details given below).

To further understand the transport properties, the cationic transference numbers for the entire series of composite electrolytes were measured at 60 °C. Prior to the transference number calculation by the Bruce-Vincent equation, EIS data was fitted using an appropriate equivalent circuit, illustrated in Fig. S10. Fig. 6a displays the current fading until reaching a steady-state for CPE30, and the inset figure shows the variation of interfacial resistance before and after polarization. The Nyquist plot for all electrolytes displays two semi-circles: the first observed at high frequency range can be assigned to the bulk response, while the second semi-circle at medium-to-low frequencies can be attributed to the Li/electrolyte interfacial response, from which the interfacial resistance is determined after fitting. Data for the filler-free SPE and all remaining CPEs are displayed in Fig. S11.

For the polymer electrolyte without ceramic filler, a T_+ value of 0.88 was obtained at 60 °C which is in good agreement with literature [64]. The variation across the series of CPE materials is shown in Fig. 6b. It can be seen that T_+ increases as a function of ceramic concentration for LLZO contents up to 30 wt%, followed by a dramatic decline at 40 wt%, and then increasing again for even higher loadings. It is also worth to mention that the increase in the fraction of free charge carriers as determined by FTIR can lead to an increase of the transference number. This is seen for CPEs up to 30 wt% of LLZO, with an exception for CPE20 which displayed the highest transference number and the lowest portion of free lithium cations. Starting from 40 wt% of ceramic particles and above, the transference number values are still fairly high but inferior compared to the SPE without ceramic filler.

It is apparent from Figs. 4b and 6b that similar trends can be seen for both transference number and total ionic conductivity for the polymer-rich CPEs. However, T_+ was observed to increase gradually with increasing LLZO contents up to 30 wt%. The lowest transference number was found at 40 wt% of LLZO. Therefore, to affirm the accuracy of the obtained T_+ value at 40 wt% of LLZO, we narrowed the ceramic content window centered around 40 wt% and performed additional measurements on CPEs with 35 and 45 wt% of LLZO. The obtained data at 35 and 45 wt% clearly follow the T_+ trend and confirm the low T_+ observed at 40 wt% of LLZO as displayed in the inset of Fig. 6b. Generally, published studies on composite electrolytes have not reported the Li-transference number as function of the ceramic filler concentration, but rather focused on comparing the T_+ between an SPE and a CPE only. In context of the ceramic-rich CPEs, we believe that the T_+ fluctuations observed from 50 wt% and above can be due to several factors, e.g. the presence of particles agglomerates that can be either fully or partially covered by Li_2CO_3, resulting thus in a cluster of carbonate-covered particles which can restrict lithium mobility in the electrolyte.

Considering that the nature of the ceramic-polymer interface is crucial for understanding ion transport properties in CPEs, their surface chemistry is necessary to explore. To this end, the pristine LLZO powder was examined by XPS; the results are displayed in Figs. S12b and S13. The data of the same samples show that the surface chemistry is not uniform. There are points where there is clearly a presence of carbon which originates from lithium carbonate, where also the intensity of characteristic peaks of both lanthanum and zirconium are very low. However, La and Zr peaks intensities are high at other parts of the same sample. This indicates a partial coverage of a surface layer of Li_2CO_3 on a certain proportion of the ceramic particles. A similar observation has previously been reported by Huo et al. for a PEO-based system [65]. Consequently, the first layers on the surface of LLZO were etched by argon sputtering, where after intense peaks of both La and Zr could be observed, while no carbon signal was detected.

Owing to the high resistivity of Li_2CO_3, its presence on the surface of LLZO particles could be one reason behind the increase of polymer-ceramic interfacial resistance, resulting in a lower overall ionic conductivity of CPEs. On the other hand, the presence of lithium carbonate on the surface of LLZO particles can also limit the ability of LLZO to act as an anion immobilizer. In other words, the Lewis acid-base interactions between TFSI anions and La^{3+} or Zr^{4+} from the ceramic filler is limited by the partial coverage of Li_2CO_3 since this obstructs the ability of LLZO to complex anions.

Li_2CO_3 is known to be spontaneously formed on the surface of LLZO due to its air sensitivity [39]. To affirm the negative effect of Li_2CO_3 on the global ionic conductivity, a control experiment was performed by employing Li_2CO_3 as a ceramic filler instead of LLZO. Three PTMC-Li_2CO_3 composite electrolytes were fabricated within three different ceramic concentrations of 10, 20 and 30 wt%. XRD patterns (Fig. S14) of the CPE with 30 wt% Li_2CO_3 confirmed the stable inclusion of Li_2CO_3 into the polymer, displaying the characteristic peaks of lithium carbonate.

Considering that the CPE with 30 wt% of LLZO displayed the highest ionic conductivity, it is interesting to focus on the conduction behavior of the analogous composite with 30 wt% of Li_2CO_3 (Fig. 7). Based on the shape of the Nyquist plot, a Debye equivalent circuit was used to determine the bulk resistance. The shape of the signal, displaying one obvious semi-circle (Fig. 7a), indicates that no conduction occurs at the interfaces between PTMC and Li_2CO_3, unless the time constants of both bulk and interfaces are almost identical and the two resulting semi-circles merge, but this is unlikely. Variation of the ionic conductivity as function of the temperature reveals that the composite with Li_2CO_3 exhibited considerably lower conductivities as compared to its equivalent with LLZO ceramic filler, thereby confirming the detrimental effect of lithium carbonate on the ionic conductivity in these hybrid electrolytes. It is also noteworthy that when increasing the Li_2CO_3 loading up to 50 wt%, the bulk resistance similarly increases (see Fig. S15). It thus seems that the Li_2CO_3 restrains the access to the pure LLZO surface, and then limits the capability of the ceramic fillers to immobilize the anions or to provide easily-accessible conduction pathways along the interfaces. Consequently, the LLZO surface coverage by Li_2CO_3 can be considered as a critical factor that suppresses ionic conduction along the inner interfaces in PTMC-LLZO CPEs.

The composite electrolyte with 30 wt% of LLZO exhibited the highest ionic conductivity, at which the interfacial transport was optimized. As a result of these findings, it can be suggested that the main objective of incorporating ceramic particles into an amorphous PTMC-based matrix is the creation of new transport pathways along the interfaces, and a possible increase of the number of free charge carriers in the system via a special salt-ceramic interaction. As far as a relative increase in ionic conductivity of CPEs was noticed compared to the pristine SPE, this is considered as a promising starting point to understand how the ceramic content can influence the transport mechanism and design more appropriate composite electrolytes with improved properties. Depending on ceramic loading, we here in Fig. 8 propose transport mechanisms that also take previous observations and findings into consideration. For the polymer-rich domains, lithium cations can be transported via the polymeric phase as well as along inner interfaces. Upon transition to the ceramic-rich domain, the same conduction pathways can be considered. However, the conduction becomes problematic and obstructed because of formation of ceramic agglomerates and the presence of more Li_2CO_3-containing interfaces.

4. Conclusions

In this work, polycarbonate-based composite electrolytes with a Li^+-conducting ceramic filler were fabricated and their ionic conduction properties as function of the filler concentration were investigated. It was observed that there is a dependence of the conductivity of

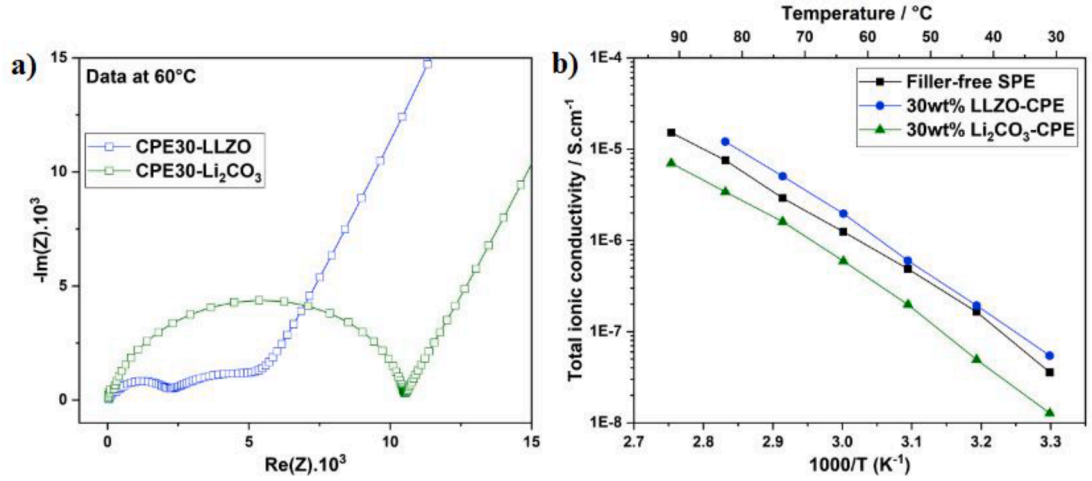

Fig. 7. (a) Nyquist plot of the composite electrolytes with 30 wt% of LLZO and Li_2CO_3 at 60 °C; (b) temperature-dependent variation of the total ionic conductivity of SPE, and CPEs with either 30 wt% of LLZO and Li_2CO_3.

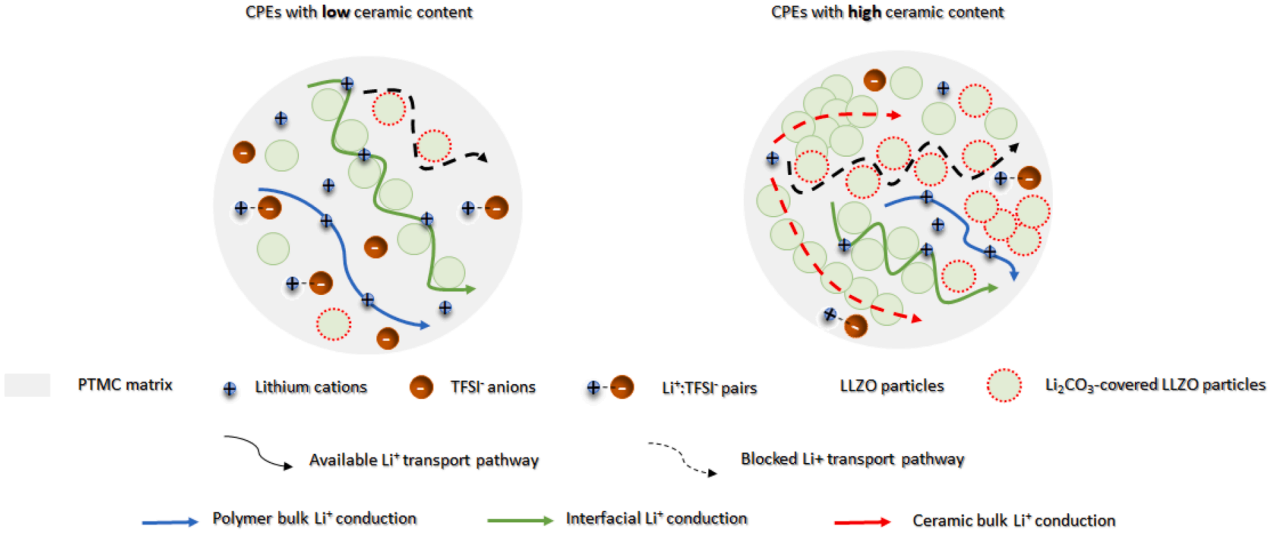

Fig. 8. Schematic representation of different possible Li-ion transport pathways in PTMC-LLZO composite electrolytes for low and high ceramic concentration. Straight and dashed lines represent the conductive and restricted ionic transport routes, respectively.

composite electrolytes with LLZO filler loadings, leading to an increase in conductivity upon addition of low-to-moderate concentrations. This increase is presumably due to the creation of an additional transport pathway along polymer-ceramic interfaces, and to an increase in the number of charge carriers in the matrix explained by a Lewis acid-base interaction between ceramic particles and lithium salt. For higher LLZO loadings, a build-up of ceramic particle agglomerates was observed, which is one factor constraining both ionic and polymer chain mobility. Importantly, the surface chemistry of the ceramic particles is shown to be vital to explain the overall conductivity of CPEs, where Li_2CO_3 coverage has detrimental effect on the ionic transport. Thereby, the incorporation of LLZO particles can lead to two opposite effects: positive for LLZO surfaces, but negative for Li_2CO_3 covered surfaces. For high LLZO contents, the negative effect of lithium carbonate is macroscopic, thus reducing the overall conductivity. Additionally, we affirm that there is no LLZO bulk transport, despite this material being considered an ion-conducting "active" ceramic filler. This study sheds light on the importance of both surface chemistry and filler loadings for the ionic conduction properties of polymer-ceramic composite electrolytes.

CRediT authorship contribution statement

Kenza Elbouazzaoui: Conceptualization, Methodology, Investigation, Writing – original draft. **Funeka Nkosi:** Investigation, Writing – review & editing. **Daniel Brandell:** Conceptualization, Methodology, Supervision, Writing – original draft, Funding acquisition. **Jonas Mindemark:** Conceptualization, Methodology, Supervision, Writing – review & editing. **Kristina Edström:** Supervision, Writing – review & editing, Funding acquisition.

Declaration of Competing Interest

The authors declare that they have no known competing financial interests or personal relationships that could have appeared to influence the work reported in this paper.

Data availability

Data will be made available on request.

Acknowledgments

This work was supported by the European Union's Horizon 2020 research and innovation program under the Marie Skłodowska-Curie grant agreement No 860403 (POLYSTORAGE), the European Research Council (ERC) under the European Horizon 2020 research and innovation program (Grant agreement No. 772777 FUN POLYSTORE), the Knut and Alice Wallenberg Foundation (INTELiSTORE 139501042) and STandUP for Energy.

Supplementary materials

Supplementary material associated with this article can be found, in the online version, at doi:10.1016/j.electacta.2023.142785.

References

[1] J.M. Tarascon, M. Armand, Issues and challenges facing rechargeable lithium batteries, Mater. Sustain. Energy (2010) 171–179, https://doi.org/10.1142/9789814317665_0024. A Collect. Peer-Reviewed Res. Rev. Artic. from Nat. Publ. Gr.
[2] A. Varzi, R. Raccichini, S. Passerini, B. Scrosati, Challenges and prospects of the role of solid electrolytes in the revitalization of lithium metal batteries, J. Mater. Chem. A 4 (2016) 17251–17259, https://doi.org/10.1039/c6ta07384k.
[3] W. Wang, Materials development for all-solid-state battery electrolytes, (2017) 203. http://hdl.handle.net/2027.42/137106.
[4] J. Mindemark, M.J. Lacey, T. Bowden, D. Brandell, Beyond PEO-Alternative host materials for Li^+-conducting solid polymer electrolytes, Prog. Polym. Sci. 81 (2018) 114–143, https://doi.org/10.1016/j.progpolymsci.2017.12.004.
[5] D. Zhou, D. Shanmukaraj, A. Tkacheva, M. Armand, G. Wang, Polymer electrolytes for lithium-based batteries: advances and prospects, Chem 5 (2019) 2326–2352, https://doi.org/10.1016/j.chempr.2019.05.009.
[6] H. Wang, L. Sheng, G. Yasin, L. Wang, H. Xu, X. He, Reviewing the current status and development of polymer electrolytes for solid-state lithium batteries, Energy Storage Mater. 33 (2020) 188–215, https://doi.org/10.1016/j.ensm.2020.08.014.
[7] J.W. Fergus, Ceramic and polymeric solid electrolytes for lithium-ion batteries, J. Power Sources 195 (2010) 4554–4569, https://doi.org/10.1016/j.jpowsour.2010.01.076.
[8] J.B. Goodenough, Ceramic solid electrolytes, Solid State Ion. 94 (1997) 17–25, https://doi.org/10.1016/s0167-2738(96)00501-2.
[9] C. Cao, Z. Bin Li, X.L. Wang, X.B. Zhao, W.Q. Han, Recent advances in inorganic solid electrolytes for lithium batteries, Front. Energy Res. 2 (2014) 1–10, https://doi.org/10.3389/fenrg.2014.00025.
[10] J.C. Bachman, S. Muy, A. Grimaud, H.H. Chang, N. Pour, S.F. Lux, O. Paschos, F. Maglia, S. Lupart, P. Lamp, L. Giordano, Y. Shao-Horn, Inorganic solid-state electrolytes for lithium batteries: mechanisms and properties governing ion conduction, Chem. Rev. 116 (2016) 140–162, https://doi.org/10.1021/acs.chemrev.5b00563.
[11] A.C. Luntz, J. Voss, K. Reuter, Interfacial challenges in solid-state Li ion batteries, J. Phys. Chem. Lett. 6 (2015) 4599–4604, https://doi.org/10.1021/acs.jpclett.5b02352.
[12] Q. Liu, Z. Geng, C. Han, Y. Fu, S. Li, Y. bing He, F. Kang, B. Li, Challenges and perspectives of garnet solid electrolytes for all solid-state lithium batteries, J. Power Sources 389 (2018) 120–134, https://doi.org/10.1016/j.jpowsour.2018.04.019.
[13] A. Ulvestad, A brief review of current lithium ion battery technology and potential solid state battery technologies, (2018). http://arxiv.org/abs/1803.04317.
[14] W. Zhao, J. Yi, P. He, H. Zhou, Solid - state electrolytes for lithium - ion batteries : fundamentals, challenges and perspectives, Electrochem. Energy Rev. 2 (2019) 574–605, https://doi.org/10.1007/s41918-019-00048-0.
[15] L. Liu, L. Chu, B. Jiang, M. Li, All-solid-state lithium batteries, Solid State Ion. 331 (2019) 89–95, https://doi.org/10.1016/j.ssi.2019.01.007.
[16] M. Keller, A. Varzi, S. Passerini, Hybrid electrolytes for lithium metal batteries, J. Power Sources 392 (2018) 206–225, https://doi.org/10.1016/j.jpowsour.2018.04.099.
[17] J. Liang, J. Luo, Q. Sun, X. Yang, R. Li, X. Sun, Recent progress on solid-state hybrid electrolytes for solid-state lithium batteries, Energy Storage Mater. 21 (2019) 308–334, https://doi.org/10.1016/j.ensm.2019.06.021.
[18] P. Yao, H. Yu, Z. Ding, Y. Liu, J. Lu, M. Lavorgna, J. Wu, X. Liu, Review on polymer-based composite electrolytes for lithium batteries, Front. Chem. 7 (2019) 1–17, https://doi.org/10.3389/fchem.2019.00522.
[19] X. Chen, P.M. Vereecken, Solid and solid-like composite electrolyte for lithium ion batteries: engineering the ion conductivity at interfaces, Adv. Mater. Interfaces 6 (2019) 1–31, https://doi.org/10.1002/admi.201800899.
[20] J. Mindemark, S. Yuan, Challenges and development of composite solid-state electrolytes for high-performance lithium ion batteries, 441 (2019). 10.1016/j.jpowsour.2019.227175.
[21] S. Xia, X. Wu, Z. Zhang, Y. Cui, W. Liu, Practical challenges and future perspectives of all-solid-state lithium-metal batteries, Chem 5 (2019) 753–785, https://doi.org/10.1016/j.chempr.2018.11.013.
[22] X. Yu, A. Manthiram, A review of composite polymer-ceramic electrolytes for lithium batteries, Energy Storage Mater. 34 (2021) 282–300, https://doi.org/10.1016/j.ensm.2020.10.006.
[23] M. Armand, M. Chabagno, J.M. Duclot, Polymeric solid electrolytes, in: Proceedings of the Second International Meeting on Solid Electrolytes, 1978, pp. 20–22. Polymeric.
[24] M. Armand, M. Chabagno, J.M. Duclot, Polyethers as solid electrolytes, in: P. Vashishta (Ed.), Fast Ion Transport in Solids: Electrodes and Electrolytes, North Holland, 1979. New York. 131.
[25] A. Manthiram, X. Yu, S. Wang, Lithium battery chemistries enabled by solid-state electrolytes, Nat. Rev. Mater. 2 (2017) 1–16, https://doi.org/10.1038/natrevmats.2016.103.
[26] Y. Jiang, X. Yan, Z. Ma, P. Mei, W. Xiao, Q. You, Y. Zhang, Development of the PEO based solid polymer electrolytes for all-solid state lithium ion batteries, Polymers 10 (2018) 1–13, https://doi.org/10.3390/polym10111237 (Basel).
[27] W. Wang, E. Yi, A.J. Fici, R.M. Laine, J. Kieffer, Lithium ion conducting poly (ethylene oxide)-based solid electrolytes containing active or passive ceramic nanoparticles, J. Phys. Chem. C 121 (2017) 2563–2573, https://doi.org/10.1021/acs.jpcc.6b11136.
[28] L. Zhu, P. Zhu, Q. Fang, M. Jing, X. Shen, L. Yang, A novel solid PEO/LLTO-nanowires polymer composite electrolyte for solid-state lithium-ion battery, Electrochim. Acta 292 (2018) 718–726, https://doi.org/10.1016/j.electacta.2018.10.005.
[29] F. Chen, D. Yang, W. Zha, B. Zhu, Y. Zhang, J. Li, Y. Gu, Q. Shen, L. Zhang, D. R. Sadoway, Solid polymer electrolytes incorporating cubic $Li_7La_3Zr_2O_{12}$ for all-solid-state lithium rechargeable batteries, Electrochim. Acta 258 (2017) 1106–1114, https://doi.org/10.1016/j.electacta.2017.11.164.
[30] B. Commarieu, A. Paolella, J.C. Daigle, K. Zaghib, Toward high lithium conduction in solid polymer and polymer–ceramic batteries, Curr. Opin. Electrochem. 9 (2018) 56–63, https://doi.org/10.1016/j.coelec.2018.03.033.
[31] L. Zr, O. Al, X. Fu, Y. Li, C. Liao, W. Gong, M. Yang, R. Kwok, Y. Li, S. Chin, Z. Lu, Enhanced electrochemical performance of solid PEO /$LiClO_4$ electrolytes, Compos. Sci. Technol. 184 (2019), 107863, https://doi.org/10.1016/j.compscitech.2019.107863.
[32] Z. Li, H.M. Huang, J.K. Zhu, J.F. Wu, H. Yang, L. Wei, X. Guo, Ionic conduction in composite polymer electrolytes: case of PEO:Ga-LLZO composites, ACS Appl. Mater. Interfaces 11 (2019) 784–791, https://doi.org/10.1021/acsami.8b17279.
[33] D. Cai, D. Wang, Y. Chen, S. Zhang, X. Wang, X. Xia, J. Tu, A highly ion-conductive three-dimensional LLZAO-PEO/LiTFSI solid electrolyte for high-performance solid-state batteries, Chem. Eng. J. 394 (2020), 124993, https://doi.org/10.1016/j.cej.2020.124993.
[34] K. He, C. Chen, R. Fan, C. Liu, C. Liao, Y. Xu, J. Tang, R.K.Y. Li, Polyethylene oxide/garnet-type $Li_{6.4}La_3Zr_{1.4}Nb_{0.6}O_{12}$ composite electrolytes with improved electrochemical performance for solid state lithium rechargeable batteries, Compos. Sci. Technol. 175 (2019) 28–34, https://doi.org/10.1016/j.compscitech.2019.02.030.
[35] Z. Bi, W. Huang, S. Mu, W. Sun, N. Zhao, X. Guo, Dual-interface reinforced flexible solid garnet batteries enabled by *in-situ* solidified gel polymer electrolytes, Nano Energy 90 (2021), 106498, https://doi.org/10.1016/j.nanoen.2021.106498.
[36] Z. Bi, Q. Sun, M. Jia, M. Zuo, N. Zhao, X. Guo, Molten salt driven conversion reaction enabling lithiophilic and air-stable garnet surface for solid-state lithium batteries, Adv. Funct. Mater. 32 (2022), https://doi.org/10.1002/adfm.202208751.
[37] M.V. Reddy, C.M. Julien, A. Mauger, K. Zaghib, Sulfide and oxide inorganic solid electrolytes for all-solid-state li batteries: a review, Nanomaterials 10 (2020) 1–80, https://doi.org/10.3390/nano10081606.
[38] C.A. Geiger, E. Alekseev, B. Lazic, M. Fisch, T. Armbruster, R. Langner, M. Fechtelkord, N. Kim, T. Pettke, W. Weppner, Crystal chemistry and stability of "Li7La 3Zr2O12" garnet: a fast lithium-ion conductor, Inorg. Chem. 50 (2011) 1089–1097, https://doi.org/10.1021/ic101914e.
[39] S. Ramakumar, C. Deviannapoorani, L. Dhivya, L.S. Shankar, R. Murugan, Lithium garnets: synthesis, structure, Li^+ conductivity, Li^+ dynamics and applications, Prog. Mater. Sci. 88 (2017) 325–411, https://doi.org/10.1016/j.pmatsci.2017.04.007.
[40] X. Xiang, Y. Liu, F. Chen, W. Yang, J. Yang, X. Ma, D. Chen, K. Su, Q. Shen, L. Zhang, Crystal structure and lithium ionic transport behavior of Li site doped $Li_7La_3Zr_2O_{12}$, J. Eur. Ceram. Soc. 40 (2020) 3065–3071, https://doi.org/10.1016/j.jeurceramsoc.2020.02.054.
[41] L. Li, Y. Deng, G. Chen, Status and prospect of garnet/polymer solid composite electrolytes for all-solid-state lithium batteries, J. Energy Chem. 50 (2020) 154–177, https://doi.org/10.1016/j.jechem.2020.03.017.
[42] D. Zhou, M. Zhang, F. Sun, T. Arlt, J.E. Frerichs, K. Dong, J. Wang, A. Hilger, F. Wilde, M. Kolek, M.R. Hansen, P. Bieker, I. Manke, M.C. Stan, M. Winter, Performance and behavior of LLZO-based composite polymer electrolyte for lithium metal electrode with high capacity utilization, Nano Energy 77 (2020), https://doi.org/10.1016/j.nanoen.2020.105196.
[43] H. Zhai, P. Xu, M. Ning, Q. Cheng, J. Mandal, Y. Yang, A flexible solid composite electrolyte with vertically aligned and connected ion-conducting nanoparticles for lithium batteries, Nano Lett. 17 (2017) 3182–3187, https://doi.org/10.1021/acs.nanolett.7b00715.
[44] L. Xu, G. Li, J. Guan, L. Wang, J. Chen, J. Zheng, Garnet-doped composite polymer electrolyte with high ionic conductivity for dendrite-free lithium batteries, J. Energy Storage 24 (2019), 100767, https://doi.org/10.1016/j.est.2019.100767.
[45] F. Langer, Synthesis and electrochemical investigation of garnet-polymer composite electrolytes for solid state batteries, (2017).

[46] T. Yang, J. Zheng, Q. Cheng, Y.Y. Hu, C.K. Chan, Composite polymer electrolytes with $Li_7La_3Zr_2O_{12}$ garnet-type nanowires as ceramic fillers: mechanism of conductivity enhancement and role of doping and morphology, ACS Appl. Mater. Interfaces 9 (2017) 21773–21780, https://doi.org/10.1021/acsami.7b03806.
[47] L. Chen, Y. Li, S.P. Li, L.Z. Fan, C.W. Nan, J.B. Goodenough, PEO/garnet composite electrolytes for solid-state lithium batteries: from "ceramic-in-polymer" to "polymer-in-ceramic, Nano Energy 46 (2018) 176–184, https://doi.org/10.1016/j.nanoen.2017.12.037.
[48] J. Popovic, D. Brandell, S. Ohno, K.B. Hatzell, J. Zheng, Y.Y. Hu, Polymer-based hybrid battery electrolytes: theoretical insights, recent advances and challenges, J. Mater. Chem. A 9 (2021) 6050–6069, https://doi.org/10.1039/d0ta11679c.
[49] M.A. Ratner, P. Johansson, D.F. Shriver, Polymer electrolytes: ionic transport mechanisms and relaxation coupling, MRS Bull. 25 (2000) 31–37, https://doi.org/10.1557/mrs2000.16.
[50] Z. Zou, Y. Li, Z. Lu, D. Wang, Y. Cui, B. Guo, Y. Li, X. Liang, J. Feng, H. Li, C. W. Nan, M. Armand, L. Chen, K. Xu, S. Shi, Mobile ions in composite solids, Chem. Rev. 120 (2020) 4169–4221, https://doi.org/10.1021/acs.chemrev.9b00760.
[51] B. Sun, J. Mindemark, K. Edström, D. Brandell, Polycarbonate-based solid polymer electrolytes for Li-ion batteries, Solid State Ion. 262 (2014) 738–742, https://doi.org/10.1016/j.ssi.2013.08.014.
[52] L. Cheng, J.S. Park, H. Hou, V. Zorba, G. Chen, T. Richardson, J. Cabana, R. Russo, M. Doeff, Effect of microstructure and surface impurity segregation on the electrical and electrochemical properties of dense Al-substituted $Li_7La_3Zr_2O_{12}$, J. Mater. Chem. A 2 (2014) 172–181, https://doi.org/10.1039/c3ta13999a.
[53] B. Sun, J. Mindemark, K. Edström, D. Brandell, Polycarbonate-based solid polymer electrolytes for Li-ion batteries, Solid State Ion. (2013) 2–6, https://doi.org/10.1016/j.ssi.2013.08.014.
[54] C. Sångeland, R. Mogensen, D. Brandell, J. Mindemark, Stable cycling of sodium metal all-solid-state batteries with polycarbonate-based polymer electrolytes, ACS Appl. Polym. Mater. 1 (2019) 825–832, https://doi.org/10.1021/acsapm.9b00068.
[55] B.J.T.S. Irvine, D.C. Sinclair, A.R. West, Electroceramics Characterisation by impedance sepctroscopy.pdf, Arch. Fr. Pediatre. 42 (1985) 575–576.
[56] R.F. Samsinger, S.O. Schopf, J. Schuhmacher, P. Treis, M. Schneider, A. Roters, A. Kwade, Influence of the processing on the ionic conductivity of solid-state hybrid electrolytes based on glass-ceramic particles dispersed in PEO with LiTFSI, J. Electrochem. Soc. 167 (2020), 120538, https://doi.org/10.1149/1945-7111/abb37f.
[57] M. Kato, K. Hiraoka, S. Seki, Investigation of the ionic conduction mechanism of polyether/$Li_7La_3Zr_2O_{12}$ composite solid electrolytes by electrochemical impedance spectroscopy, J. Electrochem. Soc. 167 (2020), 070559, https://doi.org/10.1149/1945-7111/ab8478.
[58] A. Gupta, J. Sakamoto, Controlling ionic transport through the PEO-LITFSi/LLZTO interface, Electrochem. Soc. Interface 28 (2019) 63–69, https://doi.org/10.1149/2.F06192if.
[59] H. Zhang, X. Xuan, J. Wang, H. Wang, FT-IR investigations of ion association in PEO-MSCN (M = Na, K) polymer electrolytes, Solid State Ion. 164 (2003) 73–79, https://doi.org/10.1016/j.ssi.2003.08.051.
[60] J. Zhang, J. Yang, T. Dong, M. Zhang, J. Chai, S. Dong, T. Wu, X. Zhou, G. Cui, Aliphatic polycarbonate-based solid-state polymer electrolytes for advanced lithium batteries: advances and perspective, Small 14 (2018) 1–16, https://doi.org/10.1002/smll.201800821.
[61] K. Kimura, J. Motomatsu, Y. Tominaga, Correlation between solvation structure and ion-conductive behavior of concentrated poly(ethylene carbonate)-based electrolytes, J. Phys. Chem. C 120 (2016) 12385–12391, https://doi.org/10.1021/acs.jpcc.6b03277.
[62] K. Kimura, Y. Tominaga, Understanding electrochemical stability and lithium ion-dominant transport in concentrated poly (ethylene carbonate) electrolyte, (2018) 4008–4014. 10.1002/celc.201801105.
[63] J. Mindemark, S. Tang, H. Li, L. Edman, Ion transport beyond the polyether paradigm: introducing oligocarbonate ion transporters for efficient light-emitting electrochemical cells, Adv. Funct. Mater. 28 (2018) 1–9, https://doi.org/10.1002/adfm.201801295.
[64] B. Sun, J. Mindemark, E.V. Morozov, L.T. Costa, M. Bergman, P. Johansson, Y. Fang, I. Furó, D. Brandell, Ion transport in polycarbonate based solid polymer electrolytes: experimental and computational investigations, Phys. Chem. Chem. Phys. 18 (2016) 9504–9513, https://doi.org/10.1039/c6cp00757k.
[65] H. Huo, X. Li, Y. Sun, X. Lin, K. Doyle-Davis, J. Liang, X. Gao, R. Li, H. Huang, X. Guo, X. Sun, Li_2CO_3 effects: new insights into polymer/garnet electrolytes for dendrite-free solid lithium batteries, Nano Energy 73 (2020), 104836, https://doi.org/10.1016/j.nanoen.2020.104836.